Trabajo Fin de Grado
Grado en Ingeniería de las Tecnologías Industriales
Mención en Energía

Análisis termoeconómico de un ciclo compacto de CO_2 con eyector

Autor: Andrés Morillo Navarro
Tutor y publicador: José Manuel Salmerón Lissén
Tutor: Bernardo Peris Pérez

Dpto. Ingeniería Energética
Escuela Técnica Superior de Ingeniería
Universidad de Sevilla

Sevilla, 2020

GRUPOTERMOTECNIA

Trabajo Fin de Grado
Ingeniería de las Tecnologías Industriales

Análisis termoeconómico de un ciclo compacto de CO_2 con eyector

Thermoeconomic analysis of CO_2 ejector refrigeration cycle

Autor:
Andrés Morillo Navarro

Tutor y publicador:
José Manuel Salmerón Lissén
Profesor titular

Tutor:
Bernardo Peris Pérez
Profesor ayudante doctor

Dpto. de Ingeniería Energética
Escuela Técnica Superior de Ingeniería
Universidad de Sevilla

Sevilla, 2020

Trabajo Fin de Grado:

Análisis termoeconómico de un ciclo compacto de CO_2 con eyector

Thermoeconomic analysis of CO_2 ejector refrigeration cycle

Autor:	Andrés Morillo Navarro
Tutor y publicador	José Manuel Salmerón Lissén
Tutor:	Bernardo Peris Pérez

El tribunal nombrado para juzgar el Proyecto arriba indicado, compuesto por los siguientes miembros:

Presidente:

Vocales:

Secretario:

Acuerdan otorgarle la calificación de:

Sevilla, 2020

El Secretario del Tribunal

Agradecimientos

A José Manuel por brindarme la oportunidad de hacer este trabajo, a mi profesor y tutor Bernardo por todo lo aprendido y la experiencia vivida, y a mi familia y amigos por el apoyo continuo e incodicional. Dedicado a mi madre María y mi padre Juan Luis que me han permitido llegar hasta aquí.

Andrés Morillo Navarro

Sevilla,

Resumen

Actualmente, la industria de refrigeración está adoptando una estrategia proactiva de sustitución de gases fluorados por alternativas más sostenibles con bajo potencial de efecto invernadero. El R744 es un refrigerante natural que ha sido ampliamente propuesto para aplicaciones de refrigeración comercial. Su uso en sistemas de cascada o tipo "booster" permite producir simultáneamente frío para aplicación de enfriamiento y congelación. Sin embargo, cuando únicamente se requiere una etapa de evaporación a baja temperatura, el uso del R744 en ciclos de tipo transcríticos es escasa. Los principales motivos son debidos al bajo rendimiento del ciclo (COP, por las siglas en inglés) en climas cálidos, así como las limitaciones técnicas encontradas en los compresores comerciales para alcanzar las relaciones de compresión extremas requeridas por el ciclo. A la luz de estos inconvenientes, y dada la creciente necesidad de equipos para aplicaciones de baja temperatura que utilicen fluidos sostenibles y que puedan operar en climas cálidos, este trabajo propone el uso del R744 en el Ciclo de Refrigeración con Expansión por Eyector (EERC, por las siglas en inglés). Para evaluar la viabilidad de la propuesta, este estudio lleva a cabo una evaluación termoeconómica. Para ello, se ha desarrollado un modelo completo del sistema, incluyendo un eyector bifásico, un compresor comercial de doble etapa, y se han simulado condiciones de evaporación desde -10 ºC hasta -38.5ºC, la cual se reveló como la temperatura más baja alcanzable con este sistema para evitar el punto triple dentro del eyector. La optimización se realizó utilizando el Valor Presente Neto como función objetivo. De este modo, los resultados mostraron que, en comparación con el ciclo transcrítico utilizado como sistema de referencia, el EERC permite utilizar compresores comerciales más pequeños dentro de unos límites operativos más amplios. Además, se alcanzaron mejoras del COP superiores al 22% a la vez que se reducían los costes de inversión y energéticos. Así, se puede concluir que el EERC utilizando R744 es viable para aplicaciones de producción de frio a baja temperatura en climas cálidos.

Abstract

Refrigeration industry is adopting a proactive strategy to phase out fluorinated greenhouse gases by more sustainable working fluids. R744 is a natural refrigerant widely proposed for commercial refrigeration. Its use in cascade and booster cycles allows a combined cooling and freezing production. However, when single-stage evaporation at low temperature is required, the adoption of R744 in transcritical cycles is scarce. The main reasons are due to the low Coefficient of Performance (COP) achieved, as well as the technical limitations to reach extreme pressure ratios using commercial compressors. In light of this, this study proposes to use the CO_2 Ejector-Expansion Refrigeration Cycle (EERC) to overcome these drawbacks. To assess the feasibility of the proposal, a thermoeconomic optimization is conducted for low-temperature refrigeration in warm climates. The analysis has been conducted considering a two-phase flow ejector, a commercial double-stage compressor, and evaporating conditions ranging from -10 ºC to -38.5 ºC, which was revealed the minimum temperature to avoid the triple point inside the ejector. The results showed that, compared to the reference cycle, the EERC allows using smaller commercial compressors within a broader operating envelope, improving the COP above 22% while reducing investment and yearly power costs.

Contents

iii

Agradecimientos **vii**

Resumen **ix**

Abstract **xi**

Contents **xiii**

List of Tables **xv**

List of Figures **xvii**

Nomenclature **xix**

1 Introduction **21**

2 System description **25**

3 System modeling **27**

3.1. Two-phase flow ejector *27*

3.1.1 Suction chamber 27

3.1.2 Mixing Section 29

3.1.3 Diffuser 29

3.1.4 Ejector analysis 30

3.2 Double-stage compressor *30*

3.3 Thermoeconomic analysis methodology *33*

4 Results and discussion **39**

5 Conclusions **45**

References **47**

List of Tables

Table 1-1. Low-temperature refrigeration applications using CO_2. 22
Table 3-1. List of coefficients used in the second order correlation of Eq. (22). 32
Table 3-2. Energy balance equations of the components of the cycles. 34
Table 3-3. Overall heat transfer coefficient considered. 34
Table 3-4. Investment cost correlation of the components. 35
Table 3-5. Economic and operating parameters considered. 35

List of Figures

Fig. 2-1. RC: (a) architecture with double-stage compressor, intercooler, and internal heat exchanger; (b) P-h diagram of transcritical cycle with CO_2. 25

Fig. 2-2. EERC: (a) architecture with double-stage compressor, intercooler, internal heat exchanger, and ejector-expander; (b) P-h diagram of transcritical cycle with CO_2. 26

Fig. 2-3. Not scaled phase diagram for CO_2. 26

Fig. 3-1. Schematic of ejector, pressure, and velocity profile. 28

Fig. 3-2. Operating limits of commercial CO_2 compressors: (a) gas cooler pressure vs. evaporating temperature; (b) pressure ratio vs. evaporating temperature. 30

Fig. 3-3. Black-box model of the double-stage compressor with intercooler. 31

Fig. 3-4. Operating envelope of the double-stage compressor with intercooler: white dots are used for correlations development and blue crosses are used for the model validation. 31

Fig. 3-5. Black-box model validation: (a) specific electric power absorbed by the double-stage compressor; (b) intercooler specific capacity; (c) compressor discharge temperature at the upper stage. 33

Fig. 3-6. Flowchart of the thermoeconomic optimization procedure. 37

Fig. 4-1. EERC modified envelope: (a) DORIN; (b) GEA; (c) FRASCOLD. 40

Fig. 4-2. EERC and RC thermodynamic performance: (a) COP; (b) electric power absorbed by the compressor; (c) gas cooler capacity. 42

Fig. 4-3. Ejector parameters analysis: (a) entrainment ratio; (b) Elbel's efficiency. 43

Fig. 4-4. Normalized investment cost optimizing the NPV. 44

Fig. 4-5. NPV of the EERC and RC cycle for different refrigeration capacities. 44

Nomenclature

Acronyms

A	Area (m^2)
C	Cost (€)
ce	Cost of electricity (€/kWh)
COP	Coefficient of Performance
EERC	Ejector-Expansion Refrigeration Cycle
GWP	Global Warming Potential
h	Enthalpy ($kJ \cdot kg^{-1}$)
HFC	Hydrofluorocarbon
HP	High Pressure stage
i	Interest rate (%)
IC	Intercooler
IHX	Internal Heat Exchanger
LMTD	Logarithmic Mean Temperature Difference
LP	Low Pressure stage
M	Mach number
$\dot{m}$	Mass flow rate ($kg \cdot s^{-1}$)
n	Years of operation
NPV	Net Present Value (€)
OH	Operation Hours in a year
P	Pressure (bar)
q	Specific thermal power ($kJ \cdot kg^{-1}$)
Q	Thermal power (kW)
RC	Reference cycle
s	Entropy ($kJ \cdot kg^{-1} \cdot K^{-1}$)
T	Temperature (K)
u	Velocity ($m \cdot s^{-1}$)
U	Overall heat transfer coefficient ($kW \cdot m^{-2} \cdot K^{-1}$)
$\dot{V}$	Volumetric flow rate ($m^3 \cdot s^{-1}$)
w	Specific electric power absorbed ($kJ \cdot kg^{-1}$)
W	Electric power absorbed (kW)

Greek symbols

β	Thermal expansion coefficient (K^{-1})
ε	Effectiveness
ϵ	Void fraction

η	Efficiency (%)
ρ	Density ($kg \cdot m^{-3}$)
ϕ	Efficiency due to frictional loss
ω	Entrainment ratio

Subscripts

as	After shock wave
c	Compressor
d	Diffuser of the ejector
e	Evaporator
gc	Gas cooler
i	Inlet
l	liquid phase
m	Mixed flow
o	Outlet
p	Primary fluid
p1	Primary nozzle exit
s	Secondary fluid
t	Throat of the nozzle
v	vapor phase
y	Flow at the location of choking

1 INTRODUCTION

Global warming has become one of the main social challenges in recent years. To face this problem, governments and organizations are encouraging companies to reduce greenhouse emissions through more restrictive environmental regulations. In this way, the Kigali amendment on substances that deplete the ozone layer, which came into force in 2019 by the ratification of 65 countries, aimed to reduce the HFC production and consumption to avoid a temperature increase of 0.4 ºC at the end of the century [1]. Among energy consumer sectors, the refrigeration industry highlights, whose demand is expected to be raised to 72% during the present century [2]. Furthermore, the refrigeration industry consumes tons of fluorinated refrigerants with high values of Global Warming Potential (GWP), which are intended to be gradually replaced by more sustainable alternatives. In Europe, the F-Gas Regulation is responsible for a progressive phase-out of fluorinated fluids with high GWP in refrigeration applications. According to this regulation, refrigeration systems that use working fluids with a GWP higher than 150 will be forbidden in 2020. Moreover, to accelerate this process towards the use of more friendly fluids, the European Parliament established by the Regulation No 517/2014 [3] quotas to HFCs that penalized high GWP refrigerants, aiming to reduce the F-Gases commercialization to 21% by 2030 [4].

In response to this requirement, natural refrigerants emerge as a solution with null or marginal GWP. Accordingly, refrigeration companies are now involved in a proactive strategy to fulfill the future demand with more sustainable systems. The most currently investigated natural refrigerants are ammonia (R717), hydrocarbons, and CO_2 (R744). Ammonia is currently being used in food retail applications. However, despite the suitable performance reachable using R717, its adoption is not widespread due to its toxicity [5]. Hydrocarbons, such as propane or isobutane, also achieve great performance ratios. These fluids are used in domestic and commercial systems that require minimum refrigerant charges, due to its flammability and explosion hazard [6]. CO_2 is a non-flammable, non-toxic fluid with a GWP of 1. Its production is considered simple and cheap, besides recoverable [7]. The main drawback of R744 is associated with its high discharge pressure, which exceeds the critical point in warm climates. Nonetheless, the main technical constraints related to the pressure are already overcome [8]. Indeed, many companies are promoting the R744 use for a combined cooling and freezing production. Cascade cycles can operate with CO_2 in the low-temperature circuit, and ammonia, or HFCs in the high-temperature circuit, solving problems of high-pressure operations and achieving great values of COP. Different alternatives can be found in the literature to be used as high-temperature refrigerant for cascade systems with R744, natural fluids like propane [9], fluorinated fluids such as R513A as a replacement of R134a, or pure and azeotropic mixtures of hydrofluorocarbons [10]. Furthermore, R744 can also be used in booster systems for a combined cooling and freezing production. This system operates in the subcritical cycle in cold climates and transcritical cycle in warm climates, exhibiting satisfactory performance ratios. Numerous improvements are proposed in the literature to enhance the COP of the booster cycle with R744 [11]. P. Gullo *et al.* [12] compared the booster transcritical CO_2 system with parallel compressors to the direct expansion system using R404A, concluding that the use of parallel compressors improved the COP by 30% in booster systems. This investigation stated that ejector expanders may be installed in different parts of the cycle, reducing the pressure ratio in the compressor and achieving COP improvements up to 27%, depending on the boundary conditions [13]. Recently, Zolcer *et al.* [14] demonstrated that the combination of ejectors and parallel compression in transcritical systems exhibited suitable efficiencies, with savings ranging between 8 and 10% compared to the basic transcritical system operating in warm climates. The ejector was considered a breakthrough for CO_2 refrigeration systems, which enabled to decrease the compression ratio, and allowed to reduce the compressor discharge temperature. Accordingly, Elbel *et al.* [15] used the ejector to lift the suction pressure of the compressor, obtaining reductions in the compressor consumption compared to the

basic cycle. Santini *et al.* [16] experimentally compared the CO_2 cycle to the ejector transcritical system, demonstrating reductions in the discharge temperature up to 35 K. Jin *et al.* [17] studied a CO_2 transcritical system for cooling and dehumidification, authors realized that a two-phase ejector implementation provided a COP improvement ranging between 12 and 60% in comparison to the standard cycle. Other improvements proposed for the CO_2 systems have been proven with suitable results, such as the study of Zolcer *et al.* [18], who used an adiabatic gas cooler to save between 8 and 12% of power consumption in warm climates.

When a single-stage evaporation at low temperature is required, different alternatives to R744 are generally adopted. For instance, low-temperature refrigeration is common in the food industry, exposing products to temperatures below -30 ºC for a longer preservation [19]. This application is typical in cold storage cabinets and rooms [20], freezing tunnels [21], and shipboard cold stores [22]. Typical refrigerants used in these applications are natural refrigerants such as ammonia, with the above-mentioned issue of toxicity [23], or HFC working fluids like R404A or R449A, that have high values of GWP. In other words, the R744 use for low-temperature refrigeration is associated with cascade and booster architectures, as Table 1-1 lists. The main reason why the transcritical CO_2 cycle is not commonly adopted is due to the low Coefficient of Performance (COP) achieved, especially in warm climates, besides the technical limitations of commercial compressors to reach extreme pressure ratios, which are imposed by low evaporating temperatures and high discharge pressures.

Table 1-1. Low-temperature refrigeration applications using CO_2.

Cycle typology	Te (ºC)	Working fluid	Load (kW)	COP	Tgc (ºC)	Ref.
Cascade system	-50	R717/R744	207	1.15	35	[24]
Cascade system	-56	R717/R744	267	1.13	40	[25]
Booster	-34	R744	65	1.319	46	[26]
Parallel Booster	-32	R744	25,5	1	40	[27]
Booster with ejector	-35	R744	30	1.5	35	[28]
Parallel Booster with ejector	-32	R513a/R744	41	1.5	40	[29]

Taking this into consideration, this stduy proposes the architecture of the Ejector-Expansion Refrigeration Cycle (EERC) to overcome these drawbacks for low-temperature refrigeration using R744 as working fluid in warm climates. The EERC adoption has demonstrated advantages in the literature using different refrigerants, such as the reduction of power consumption, lower discharge temperatures, and better values of COP compared to the basic cycle. For instance, Deng *et al.* [30] studied the EERC system for air conditioning applications, reporting a COP improvement of 22% with respect to the conventional vapor compression cycle. Yari *et al.* [31] tested an EERC demonstrating the compression ratio reductions, lower values of discharge temperature, and improvements in the COP up to 21%. The basic EERC is also able to be improved when increasing the subcooling degree. In this way, Bai *et al.* [32] analyzed the transcritical two-stage CO_2 cycle with a split-cycle for subcooling, reaching performance improvements up to 7.7%. Recently, Liu *et al.* [33] studied the EERC using a thermoelectric subcooling that improved the COP by 39.34%.

To assess the thermodynamic and economic feasibility of the proposal, a thermoeconomic optimization of the CO_2 EERC is conducted for low-temperature refrigeration in warm climates. The model of the system is developed considering a two-phase flow ejector, a double-stage compressor with intercooler, and an internal heat exchanger for superheating-subcooling. As a novelty, this investigation examines the maximum operating limits of the EERC considering thermodynamic bounds, such as the triple point of the R744 inside the ejector, and the technical restrictions of the

operating envelope of commercial compressors. Thereby, the influence of the proposal over the COP, total investment cost, and Net Present Value (NPV) will be revealed.

The rest of the document is organized as follows. Section 2 describes the proposed transcritical CO_2 EERC for low-temperature refrigeration. Section 3 describes the thermodynamic and economic model developed to conduct the analysis. Section 4 shows the optimization and discusses the results of the study. And finally, Section 5 summarizes the main conclusions of the document.

2 SYSTEM DESCRIPTION

This study proposes the use of R744 for low-temperature refrigeration in warm climates employing the EERC architecture. This cycle configuration allows reducing the pressure ratio in the compressor, which represents the main drawback to overcome in this study. Notice that, according to the previous review, the evaporating temperature of low-temperature refrigeration is around -30 ºC (14.3 bar), and the use of R744 in warm climates requires to operate in transcritical conditions, reaching discharge pressures above 73.8 bar. Besides the extreme pressure ratio that may support the compressor, which is analyzed in the forthcoming section, the high value of discharge temperature is also a constraint that requires technical solutions. Different possibilities to reduce the compressor discharge temperatures can be found in the literature [34]. The most common solution is the introduction of an intercooler between the two compression stages since it is a simple, cost-effective, and reliable method. In this way, Chen et al. [35] conducted an experimental investigation that demonstrated a 23% reduction in the discharge temperature by using the intercooler in the CO_2 refrigeration system. Manjili et al. [36] tested an intercooler between the two compression stages of the EERC that decreased the exergy destruction rate of the compressors by 60.89%. Furthermore, the adoption of an intercooler in a double-stage compressor can also improve the COP of the transcritical CO_2 refrigeration cycle, such as Wang et al. [37] demonstrated.

Accordingly, the compression process considered in the study also includes a double-stage compressor with intercooler (IC). The architecture of the basic system is shown in Fig. 2-1.a, which is considered as Reference Cycle (RC) for comparisons. The Internal Heat Exchanger (IHX) is used to avoid liquid droplets in the suction port of the compressor, ensuring a superheating degree. At the same time, the IHX provides a subcooling at the outlet of the gas cooler, which increases the vaporization enthalpy, as can be appreciated in Fig. 2-1.b. This figure also depicts the reduction of the discharge temperature using the double-stage compressor with intercooler.

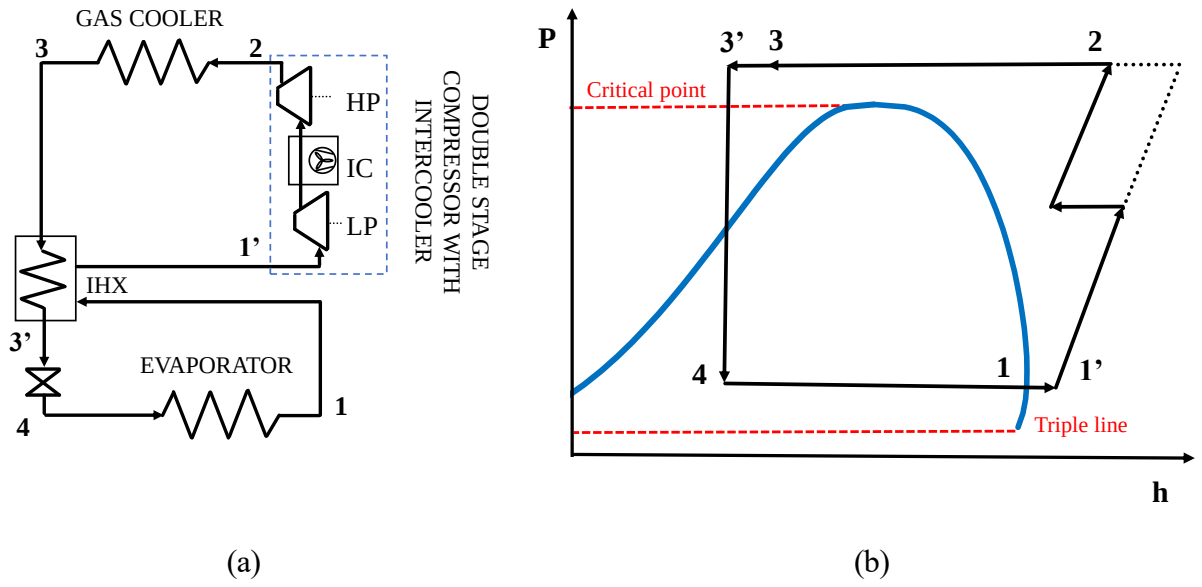

(a) (b)

Fig. 2-1. RC: (a) architecture with double-stage compressor, intercooler, and internal heat exchanger; (b) P-h diagram of transcritical cycle with CO_2.

The RC can be further improved by adopting the ejector-expander. EERC architecture is shown in Fig. 2-2.a, which illustrates that the suction from the evaporator is now conducted by the secondary nozzle of the ejector, the fluid from the gas cooler is used as the primary flow to drive the ejector,

and both flows are again divided in two-phases in the separator. As a result, Fig. 2-2.b shows that the suction temperature in the compressor (1) differs from the outlet temperature of the evaporator (6). First, this means that the discharge temperature of the compressor (2) may be lower compared to the reference cycle, assuming the same intercooler capacity. Second, the suction pressure of the compressor is higher than the evaporating pressure, reducing the compression ratio. Both simultaneous effects, reduction of discharge temperature and pressure ratio may allow the use of commercial compressors in a broader operating envelope, enabling the possibility to use the EERC with CO_2 for low-temperature refrigeration in warm climates with a suitable COP.

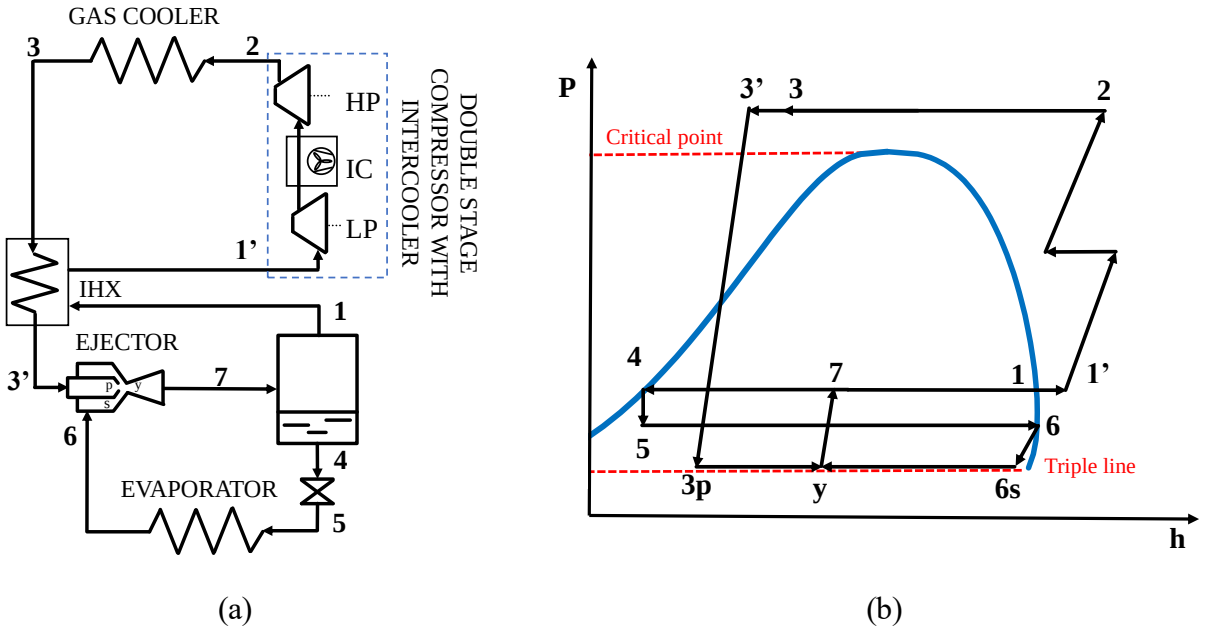

Fig. 2-2. EERC: (a) architecture with double-stage compressor, intercooler, internal heat exchanger, and ejector-expander; (b) P-h diagram of transcritical cycle with CO_2.

Besides the restrictions of the compressors operating envelope, the use of the EERC also requires paying attention to the limits in the ejector. In particular, the minimum temperature in the cycle is not obtained in the evaporator, but in the ejector as Fig. 2b shows. The thermodynamic bound corresponds to the triple point temperature, as illustrated in the phase diagram of Fig. 2-3. Therefore, the minimum evaporating temperature of the cycle must ensure temperatures inside the ejector above the triple point.

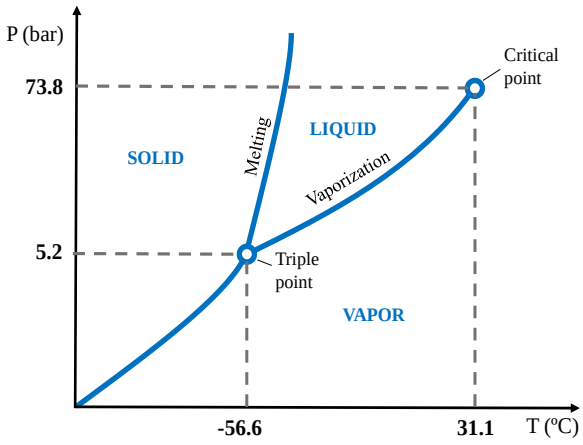

Fig. 2-3. Not scaled phase diagram for CO_2.

3 SYSTEM MODELING

To analyze the feasibility of the EERC for low-temperature refrigeration in warm climates, a thermodynamic and economic model of the system is required. This section describes the mathematical equations of the two-phase flow ejector, the black-box model developed regarding the commercial double-stage compressor with intercooler, and the methodology proposed to conduct the thermo-economic optimization.

3.1. Two-phase flow ejector

The ejector is an expansion device with no moving elements, that has been proven as cost-effective, reliable, and with an energy efficiency comparable to expanders [38]. Its operating principle is shown in Fig. 3-1. The high-pressure liquid is accelerated in the primary nozzle over the speed of sound. The low-pressure vapor enters the secondary chamber owing to the Venturi effect and mixes with the primary stream in the mixing section. A set of oblique shock waves take place to adapt the flow to subsonic conditions before the difusser, rising the pressure at the same time. Specifically, in 1-D models this set of shock waves is usually modelled as a normal shock wave. Furthermore, deceleration of mixed streams occurs in the diffuser, converting kinematic energy into pressure-flow work. As a result, the stream leaves the ejector in a two-phase state with a higher pressure than the secondary fluid.

The ejector modeling is based on equations gathered by Expósito et al. [39], adapted to the two-phase speed of sound calculations. The following hypotheses are also considered:

- One-dimensional and steady flow inside the ejector.
- Kinematic energy at suction and discharge ports is negligible.
- Frictional and heat losses are considered through empirical coefficients, which are generally considered above 0.9 according to values reviewed by Zhang et al. [40].
- Pressure before the choking phenomenon remains constant in the mixing chamber.
- Entropy keeps constant inside the nozzle.

3.1.1 Suction chamber

The suction chamber is composed of the primary and secondary nozzles. Primary nozzle, in turn, has a converging and diverging section, composed by the primary fluid port (p0), throat (t), and primary nozzle exit (p1). The mass and energy conservation in this section is expressed by Eq. (1) and Eq (2), respectively, where η_p represents the energy losses of the primary fluid during the process.

$$\dot{m}_p = \rho_t \cdot A_t \cdot u_t = \rho_{p1} \cdot A_{p1} \cdot u_{p1} \tag{1}$$

$$h_{po} = h_t + \frac{u_t^2}{2\eta_p} = h_{p1} + \frac{u_{p1}^2}{2} \tag{2}$$

During the expansion process, the fluid reaches the sonic velocity. Considering that R744 in transcritical conditions are entering in the primary nozzle, the sonic velocity may occur inside the liquid-vapor region. The critical velocity at chocked flow conditions has a non-linear dependency of the mixture quality, the two-phase flow pattern, and the slip between liquid and gas phase velocities [41]. Angielczyk et al. [42] suggested the Homogeneous Relaxation Model (HRM) to predict the speed of sound in the two-phase region of CO_2, which resulted much more consistent than the Homogeneous Equilibrium Model (HEM). Therefore, the model proposed by Lund and Flatten [43]

is used.

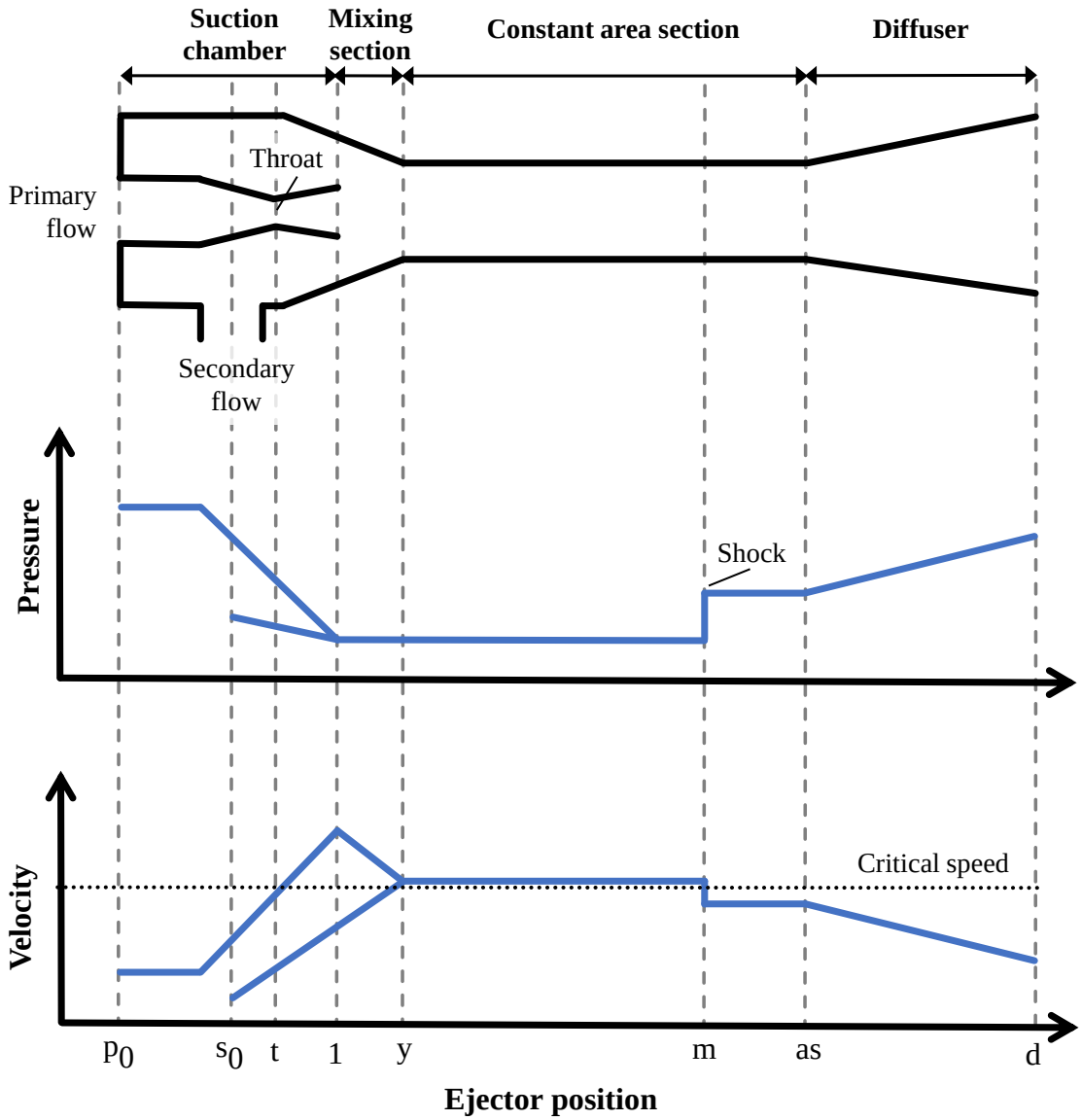

Fig. 3-1. Schematic of ejector, pressure, and velocity profile.

$$a^{-2} = a_w^{-2} + \frac{\rho}{T} \cdot \frac{C_{p,v} \cdot C_{p,l}(\zeta_l - \zeta_v)^2}{C_{p,v} + C_{p,l}} \tag{3}$$

$$a_w^{-2} = \rho \cdot \left(\frac{\epsilon_v}{\rho_v \cdot a_v^2} - \frac{\epsilon_l}{\rho_l \cdot a_l^2}\right) \tag{4}$$

$$\zeta_k = \left(\frac{\partial T}{\partial \rho}\right) = \frac{T \cdot \beta_k \cdot v_k}{c_{p,k}} \tag{5}$$

$$C_{p,k} = \rho_k \cdot \epsilon_k \cdot c_{p,k} \tag{6}$$

The mass and energy conservation of the suction chamber is expressed as Eq. (7) and Eq. (8), where ϕ_p is the primary fluid loss factor, which considers the friction effect and system inefficiencies.

$$\dot{m}_p = \rho_{py} \cdot \phi_p \cdot A_{py} \cdot u_{py} \tag{7}$$

$$h_{po} = h_{py} + \frac{u_{py}^2}{2} \tag{8}$$

Eq. (9) is the mass conservation equation for the entrained flow, which reaches the chocking conditions after the mixing process. The energy conservation is expressed by Eq. (10), where u_{sy} is the critical speed of the secondary stream at two-phase conditions by Eq. (11), and η_s represents the energy losses produced during the process.

$$\dot{m}_s = \rho_{sy} \cdot A_{sy} \cdot u_{sy} \tag{9}$$

$$h_{so} = h_{sy} + \frac{u_{sy}^2}{2\eta_s} \tag{10}$$

$$M_{sy} = \frac{u_{sy}}{a_{sy}} = 1 \tag{11}$$

3.1.2 Mixing Section

Both streams are mixed by an isobaric process, reaching a final velocity higher than the critical velocity of the fluid. The effective area of the mixing chamber remains constant according to Eq. (12). Mass, momentum, and energy conservation are obtained by Eq. (13) to Eq. (15), where ϕ_m is the mixing loss factor, which is generally considered about 0,9 for ejector devices [44].

$$A_m = A_{sy} + A_{py} \tag{12}$$

$$\dot{m}_m = \dot{m}_p + \dot{m}_s = \rho_m \cdot A_m \cdot u_m \tag{13}$$

$$\phi_m \cdot (\dot{m}_p \cdot u_{py} + \dot{m}_s \cdot u_{sy}) = \dot{m}_m \cdot u_m \tag{14}$$

$$\dot{m}_p \cdot \left(h_{py} + \frac{u_{py}^2}{2}\right) + \dot{m}_s \cdot \left(h_{sy} + \frac{u_{sy}^2}{2}\right) = \dot{m}_m \cdot \left(h_m + \frac{u_m^2}{2}\right) \tag{15}$$

The static pressure of the mixed streams increases after the shock wave, while the velocity decreases below the critical speed. The shock wave is commonly expressed in terms of thermodynamic variables by Rankine-Hugoniot equations [45]. Thus, Eq. (16) to Eq. (18) are used to address the section after the shock wave.

$$\rho_{as} \cdot u_{as} = \rho_m \cdot u_m \tag{16}$$

$$P_{as} + \rho_{as} \cdot u_{as}^2 = P_m + \rho_m \cdot u_m^2 \tag{17}$$

$$h_{as} + \frac{u_{as}^2}{2} = h_m + \frac{u_m^2}{2} \tag{18}$$

3.1.3 Diffuser

The mixed stream decelerates at the diffuser, converting the kinematic energy into pressure-flow work. In this manner, the pressure that leaves from the ejector has a higher value than the pressure of

the secondary fluid. Considering an isentropic compression, the enthalpy can be obtained by Eq. (18).

$$h_d = h_{as} + \frac{u_{as}^2}{2} \tag{19}$$

3.1.4 Ejector analysis

The entrainment ratio and the expansion efficiency are the most common parameters used to describe the ejector performance. The entrainment ratio is defined by Eq. (20) as the relationship between secondary and primary fluid mass flow rates.

$$\omega = \frac{\dot{m}_s}{\dot{m}_p} \tag{20}$$

Eq. (21) was proposed by Elbel et al. [46] as a measure of ejector efficiency. This expression is defined as the ratio between power recovered or used to compress the secondary fluid, and power produced during the expansion of the primary fluid.

$$\eta_{elbel} = \omega \cdot \frac{h_{(P_7, s_6)} - h_6}{h_3 - h_{(P_7, s_3)}} \tag{21}$$

3.2 Double-stage compressor

The adoption of a transcritical CO_2 cycle for low-temperature refrigeration requires an extreme compression ratio, not supported by standard single-stage compressors. Double-stage compressors are commercially available to operate with higher pressure ratios. However, the operating envelope of double-stage R744 compressors is still too constrained for low-temperature refrigeration in warm climates. Fig. 3-2.a shows the broader operating envelope of double stage-compressors found from a review of the main compressor manufacturers. As can be seen, the lower the evaporating temperature, the lower the discharge pressure allowed. At low evaporating temperatures, high compression ratios occur as Fig. 3-2.b shows, which represents a technical challenge for commercial compressors. Therefore, the combination of CO_2 EERC with a double-stage compressor could be a feasible solution for the application analyzed.

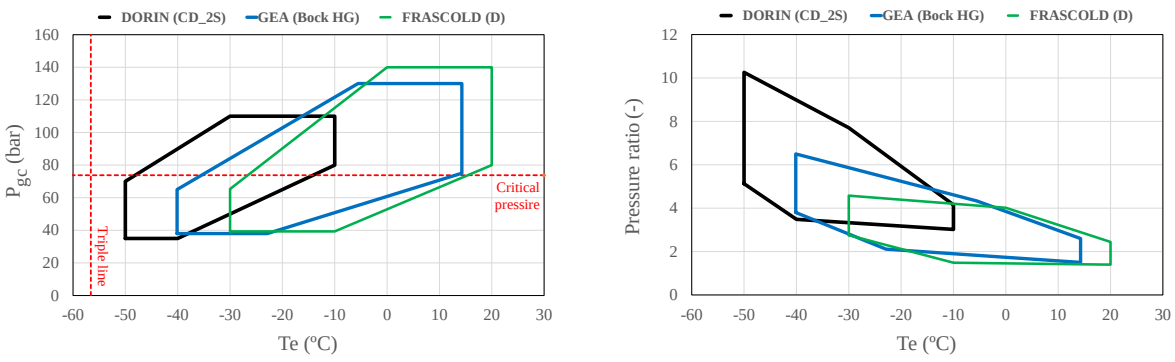

(a) (b)

Fig. 3-2. Operating limits of commercial CO_2 compressors: (a) gas cooler pressure vs. evaporating temperature; (b) pressure ratio vs. evaporating temperature.

In this study, the EERC is compared to the RC in extreme operating conditions. To assess the compressor performance in both cycles, a model of the commercial compressor that allows the broader operating conditions is developed. In particular, a black-box model of the double-stage compressor that corresponds to DORIN manufacturer is developed. Nonetheless, the analysis will also be extrapolated to the remainder operating envelopes. The black-box model proposed encompasses the double-stage compressor, including the use of the intercooler, as Fig. 3-3 depicts. This model provides the specific electric power absorbed by the double-stage compressor, the intercooler specific capacity, and the discharge temperature of the upper compression stage (HP). For the model development, a widespread simulation within the operating envelope of the compressor was conducted using the commercial software provided by the manufacturer [47]. Operating conditions used for simulations are represented in Fig. 3-4 by white dots, while operating conditions used for the model validation are represented as blue crosses. In addition, it is considered that the intercooler uses outdoor air to reject the waste heat, so it is assumed that the leaving temperature from the intercooler and gas cooler matches.

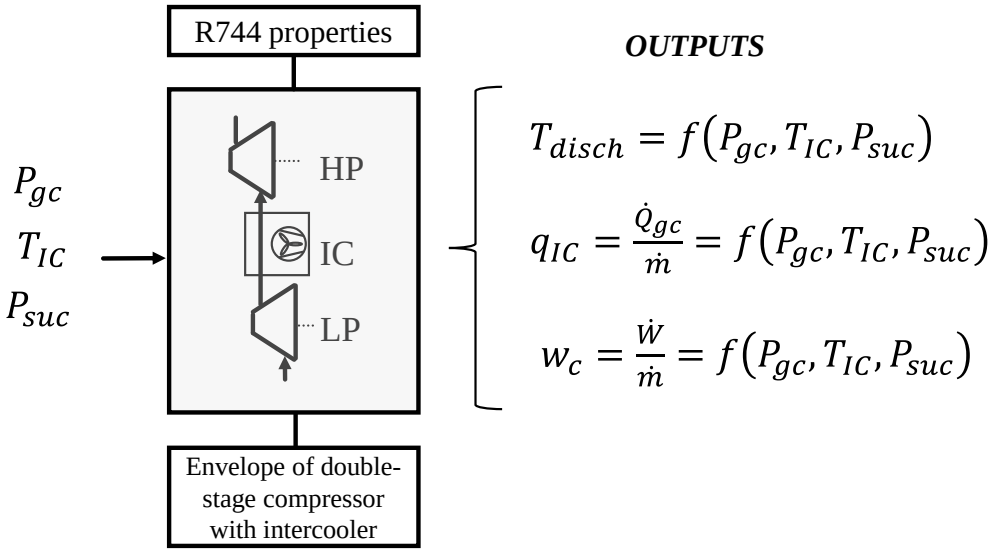

Fig. 3-3. Black-box model of the double-stage compressor with intercooler.

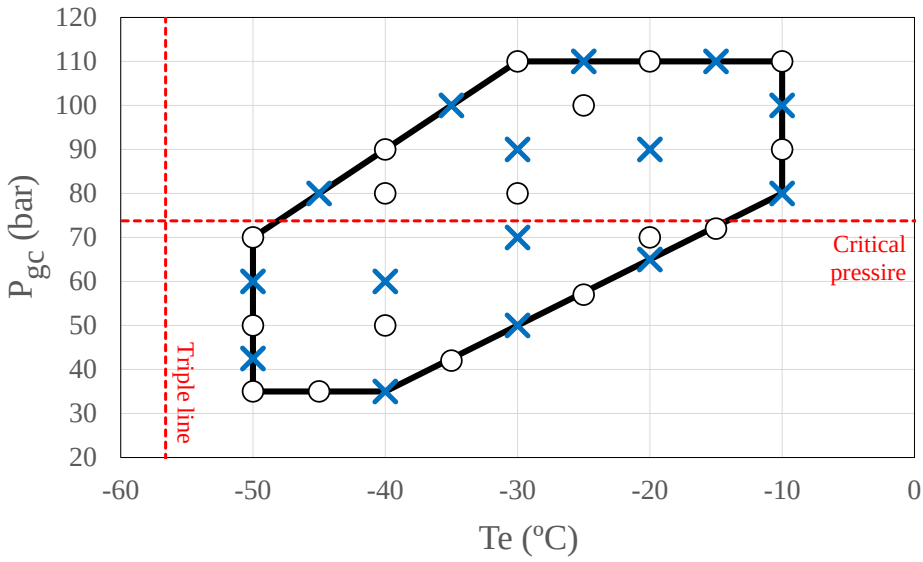

Fig. 3-4. Operating envelope of the double-stage compressor with intercooler: white dots are used for correlations development and blue crosses are used for the model validation.

The outputs of the model are set as second-order correlations to achieve suitable values of R^2. The correlation for each output (k) is shown in Eq. (22), whose coefficients and respective R^2 are collected in Table 3-1. Moreover, Fig. 3-5 represents the accuracy of the model by validating its prediction using operating conditions different from the ones used to set the correlations.

$$k = a_0 + a_1 \cdot P_{suc} + a_2 \cdot P_{gc} + a_3 \cdot T_{IC} + a_4 \cdot P_{suc}^2 + a_5 \cdot P_{gc}^2 + a_6 \cdot T_{IC}^2 + a_7 \cdot P_{suc} \cdot P_{gc} + a_8 \cdot P_{suc} \cdot T_{IC} + a_9 \cdot P_{gc} \cdot T_{IC} \quad (22)$$

Table 3-1. List of coefficients used in the second order correlation of Eq. (22).

k	w_c (kJ/kg)	q_{IC} (kJ/kg)	T_{disch} (ºC)
a_0	138.94	42.21	-46.65
a_1	-16.58	20.89e-1	-11.41
a_2	39.79e-1	-85.90e-3	52.4e-1
a_3	37.89e-1	-15.09e-1	87.03e-1
a_4	23.30e-2	-68.88e-3	21.42e-2
a_5	-11.14e-3	-40.87e-5	-75.92e-4
a_6	20.14e-2	-24.49e-3	39.91e-2
a_7	14.80e-3	48.04e-4	10.54e-3
a_8	-21.62e-3	17.40e-3	-55.01e-3
a_9	-14.79e-2	22.66e-3	-31.77e-2
R^2	99.46e-2	89.38e-2	99.89e-2

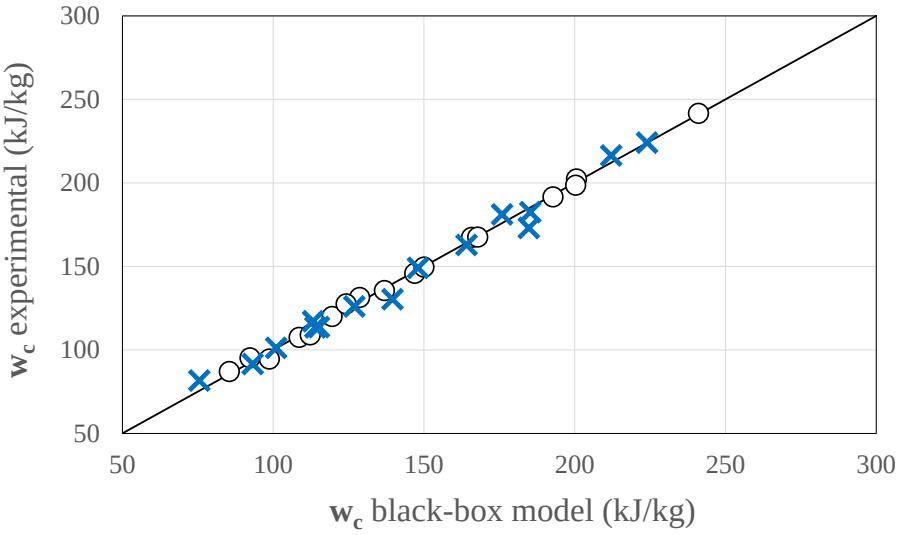

(a)

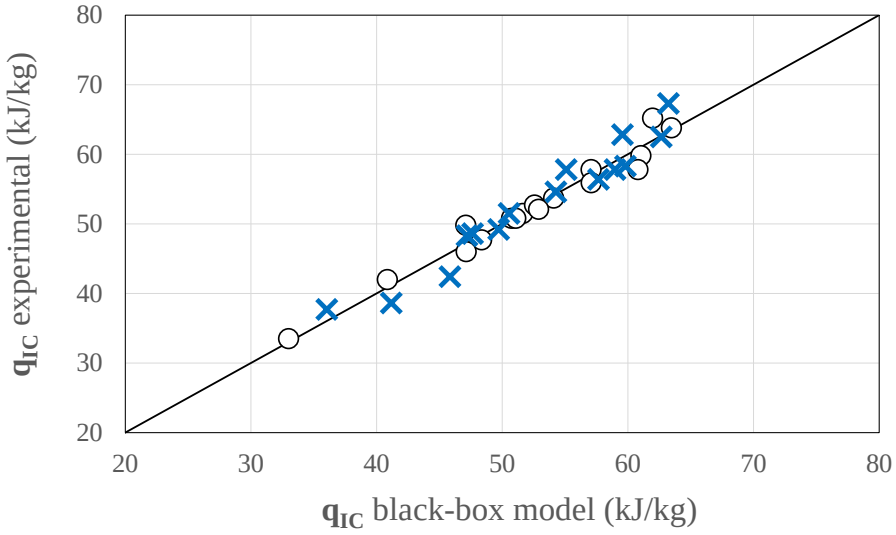

(b)

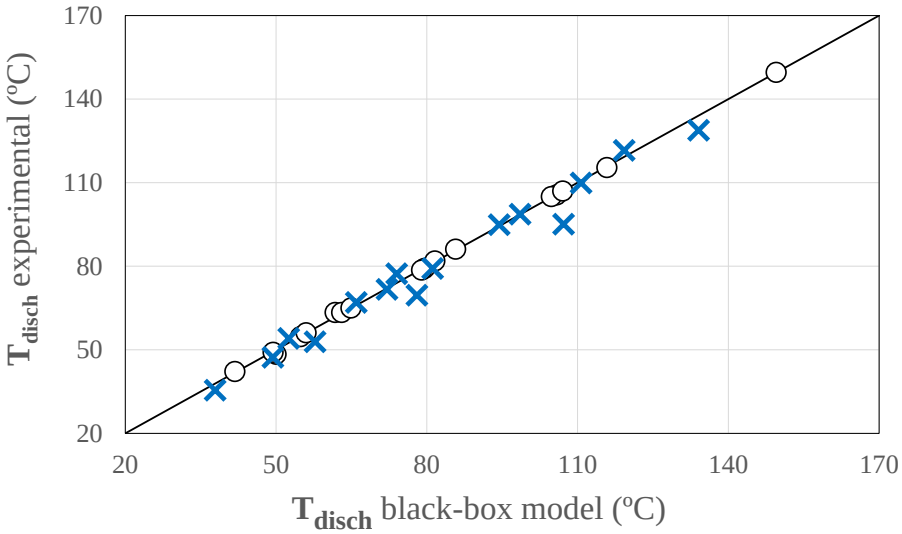

(c)

Fig. 3-5. Black-box model validation: (a) specific electric power absorbed by the double-stage compressor; (b) intercooler specific capacity; (c) compressor discharge temperature at the upper stage.

3.3 Thermoeconomic analysis methodology

The thermodynamic model is developed considering energy balances in each component of the cycle. The main equations used for the evaporator, gas cooler, internal heat exchanger, compressor, and intercooler are collected in Table 3-2.

Table 3-2. Energy balance equations of the components of the cycles.

Component	Cycle	Energy balance equation	Eq.
Evaporator	EERC	$Q_e = \dot{m}_s \cdot (h_6 - h_5)$	(23)
	RC	$Q_e = \dot{m}_T \cdot (h_1 - h_4)$	(24)
Gas cooler	EERC	$Q_{gc} = \dot{m}_p \cdot (h_2 - h_3)$	(25)
	RC	$Q_{gc} = \dot{m}_T \cdot (h_2 - h_3)$	(26)
Internal heat exchanger	EERC/RC	$\varepsilon_{IHX} = \frac{T_{1,} - T_1}{T_3 - T_1}$	(27)
		$h_{1,} - h_1 = h_3 - h_{3,}$	(28)
Compressor	EERC	$W_c = \dot{m}_p \cdot w_c$	(29)
	RC	$W_c = \dot{m}_T \cdot w_c$	(30)
Intercooler	EERC	$Q_{IC} = \dot{m}_p \cdot q_{IC}$	(31)
	RC	$Q_{IC} = \dot{m}_T \cdot q_{IC}$	(32)

Considering that both cycles, EERC and RC, are compared within the same boundary conditions, the size of each component can be calculated to assess the respective total investment cost. Thus, according to the operating limits, the IHX effectiveness defined by Eq. (27) could be optimized using as restriction the maximum discharge temperature of the compressor. The heat transfer area can be obtained from the thermal load and the LMTD method by Eq. (33) and (34). The overall heat transfer coefficients are assumed from the commercial software and those values reported in the literature, as Table 3-3 shows.

$$Q = U \cdot A \cdot LMTD \tag{33}$$

$$LMTD = \frac{(T_{hi} - T_{co}) - (T_{ho} - T_{ci})}{ln\left(\frac{T_{hi} - T_{co}}{T_{ho} - T_{ci}}\right)} \cdot F \tag{34}$$

Table 3-3. Overall heat transfer coefficient considered.

Heat exchanger	Type	$U\left(\frac{W}{m^2 \cdot K}\right)$	Ref
Evaporator	Crossflow heat exchanger	50	
Gas cooler	Crossflow heat exchanger	40	[48]
Intercooler	Crossflow heat exchanger	40	
Internal heat exchanger	Brazed plate heat exchanger	180	[49]

Thermodynamic performance and investment costs are analyzed simultaneously to reach the optimum design by a thermoeconomic analysis. To establish the total investment cost of the system, individual costs of the components are needed. The cost correlations used for the main components of the cycles are collected in Table 3-4. With regard to the compressor Eq. (35) is used, which has been developed from the budget of the commercial compressor. In particular, the displacement volume has been considered as the parameter that most influences the cost of the compressor. The ejector cost correlation has been obtained from the literature as Eq. (36), which directly depends on its operating conditions. The correlations used to obtain the costs of the heat exchangers use the heat transfer area as the main parameter, which were obtained using commercial costs and equations reported in literature, from Eq. (37) to Eq. (40). Other investment costs, related to fitting and piping, control devices, or refrigerant cost, are considered by Eq. (41).

Table 3-4. Investment cost correlation of the components.

Component	Cost correlation	Eq.	Ref.
Compressor	$C_{comp} = 4727.31 + 1122.02 \cdot \dot{V}_{dis}$	(35)	[47]
Ejector	$C_{ejector} = 15962 \cdot \dot{m} \left(\frac{T_3}{0.0001 \cdot P_3}\right)^{0.05} \cdot \left(\frac{P_7}{10}\right)^{-0.75}$	(36)	[50]
Evaporator	$C_e = 2465.96 + 96.39 \cdot A$	(37)	[48]
Internal heat exchanger	$C_{IHX} = 190 + 310 \cdot A$	(38)	[51]
Intercooler	$C_{IC} = 1397 \cdot A^{0.89}$	(39)	[49]
Gas cooler	$C_{gc} = 1397 \cdot A^{0.89}$	(40)	[49]
Miscellaneous	$C_{other} = 1.3 \sum C_x$	(41)	[51]

To achieve the most cost-effective EERC an objective function that optimizes the efficiency of the system while reduces the investment and yearly power costs is required. In this case, the Net Present Value (NPV) has been considered the variable to be maximized. Some assumptions in the optimization process have been considered, which are collected in Table 3-5.

Table 3-5. Economic and operating parameters considered.

Economic parameters	Value	Units
Interest rate (i)	5	%
Operation years (n)	20	years
Operation Hours in a year (OH)	4000	h
Cost of electricity (ce)	0.1	€/kWh

The thermoeconomic process of optimization is illustrated in Fig. 3-6. This flowchart shows thermodynamic and economic inputs to the process. The thermodynamic model starts assuming three iterative variables, which are the pressure of the gas cooler, the IHX effectiveness, and the initial ejector efficiency.

The model of the EERC and the model of the two-phase flow ejector are independently solved. The

ejector efficiency calculated according to initial values is then upgraded in the cycle, starting an iterative process until the initial and final efficiencies of the ejector converge. Notice that the ejector efficiency sets the pressures of the cycle that, in turn, are used in the model of the ejector to solve critical velocities of the fluid and the final Elbel efficiency, requiring an iterative resolution. The IHX effectiveness is optimized using as restriction the maximum discharge temperature of the compressor according to the limits of the operating envelope.

As a result, the performance of the system and size ratios of the components are obtained. These results along with the operating conditions of the refrigeration process, such as operating hours or the average cost of electricity, are used to estimate the total investment cost of the cycle and then, the NPV value. It should be noted that greater gas cooler pressures require a greater electric consumption in the compressor, which reduces the value of the COP. However, the efficiency of the ejector increases with such pressure, lifting the suction pressure of the compressor and reducing its pressure ratio. In other words, as the pressure in the gas cooler increases, the ejector efficiency also increases, but the theoretical cycle efficiency decreases. So, a thermoeconomic optimization using the NPV is required to achieve the most cost-effective solution.

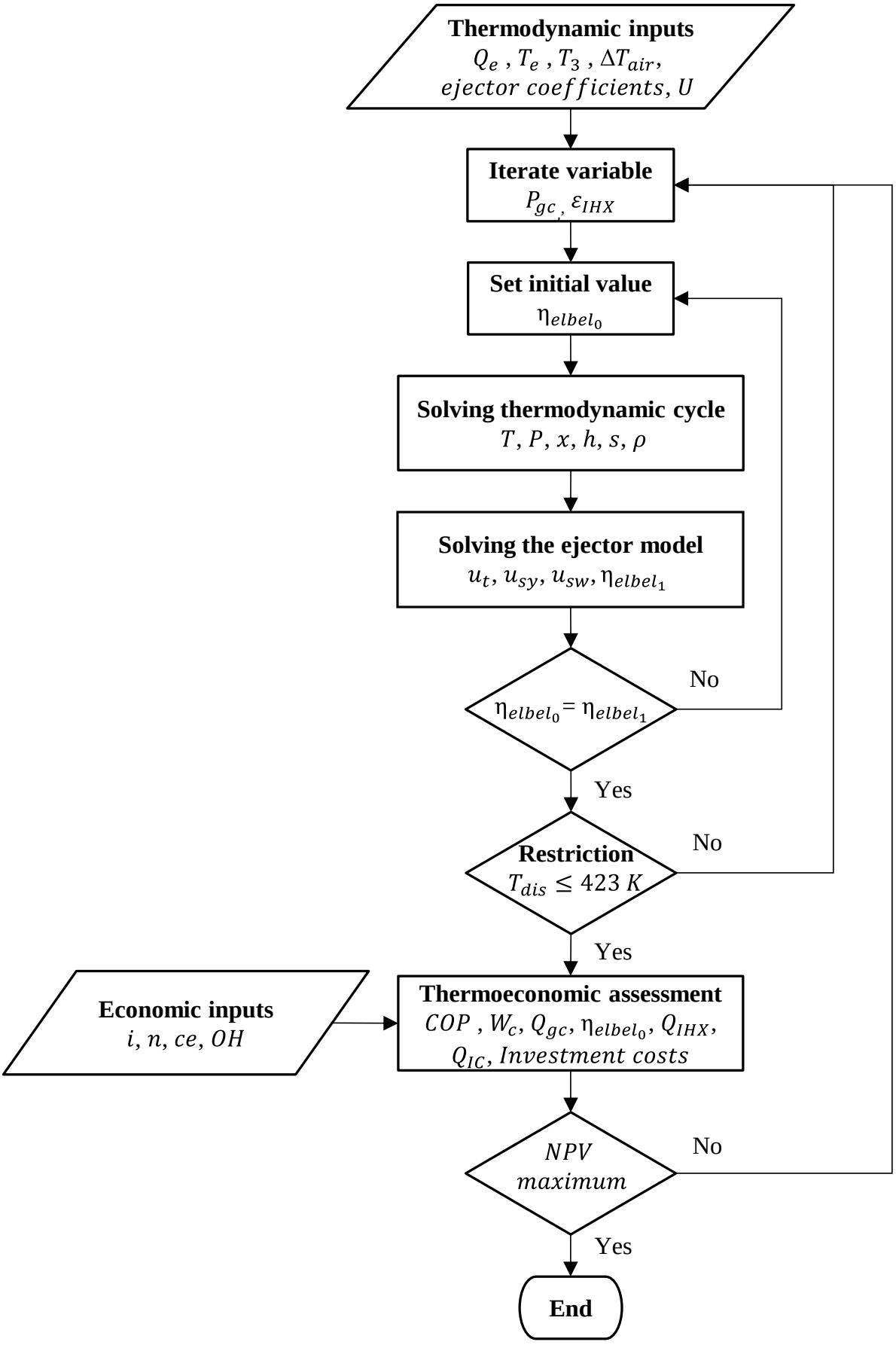

Fig. 3-6. Flowchart of the thermoeconomic optimization procedure.

4 RESULTS AND DISCUSSION

This document aims to analyze the possibilities of using the CO_2 EERC for low-temperature refrigeration in warm climates. The extreme pressure ratio to be supported by the compressor in this application represent a technical challenge for commercial compressors. However, as it was previously mentioned, the combination of the EERC with a double-stage compressor could enable that possibility. Thus, the first analysis is conducted based on the operating envelope of the cycle.

Fig. 4-1.a shows the original operating envelope of the commercial compressor with the reference cycle and the new limits achieved using the EERC. First, the minimum evaporating temperature reached is -38.5 ºC, which corresponds to a temperature inside the ejector close to the triple point. Thus, this temperature must be considered as the minimum possible using the EERC for low-temperature refrigeration. Using the EERC, the actual suction pressure does not correspond to the evaporating pressure, but the pressure leaving the ejector. Therefore, the overall operating envelope of the cycle can be expanded maintaining the pressure ratio and discharge pressure within the operating envelope of the compressor. Thus, maintaining evaporating temperatures above -38.5 ºC, discharge pressures up to 110 bar are allowed, which represent a 16.4% of improvement.

Fig. 4-1.b represents the second compressor with its original envelope, that restrings the evaporating temperature to -40 ºC. Once again, this operating map is limited by the pressure ratio, as well as suction and discharge pressure and temperatures. Through the EERC the operating envelope can be extended, increasing the discharge pressure up to 29.5% for the evaporating temperature of -38.5 ºC. This improvement means that this compressor also could be used in warm climates, offering new possibilities of application.

The most favorable compressor envelope for the use of the EERC is those whose minimum evaporating temperature is greater than -38.5 ºC. In those cases, the EERC enables reducing the evaporating temperature while allows higher dissipation temperatures. This scenario corresponds to the third compressor, which is illustrated in Fig. 4-1.c. Notice that, despite the evaporating temperature of the original compressor is limited to -30 ºC and the discharge pressure corresponds to subcritical conditions, the same compressor could be used in the EERC achieving evaporating temperatures of -38.5 ºC and operating in warm climates with transcritical conditions.

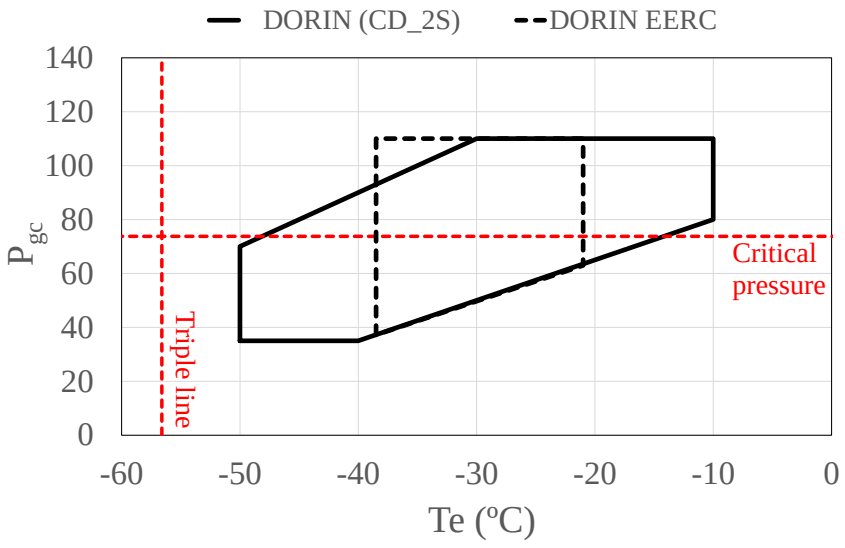

a)

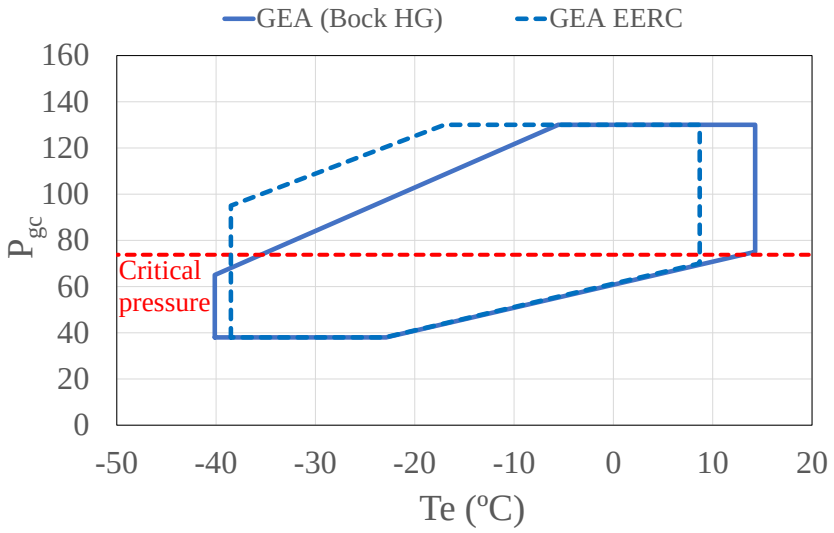

b)

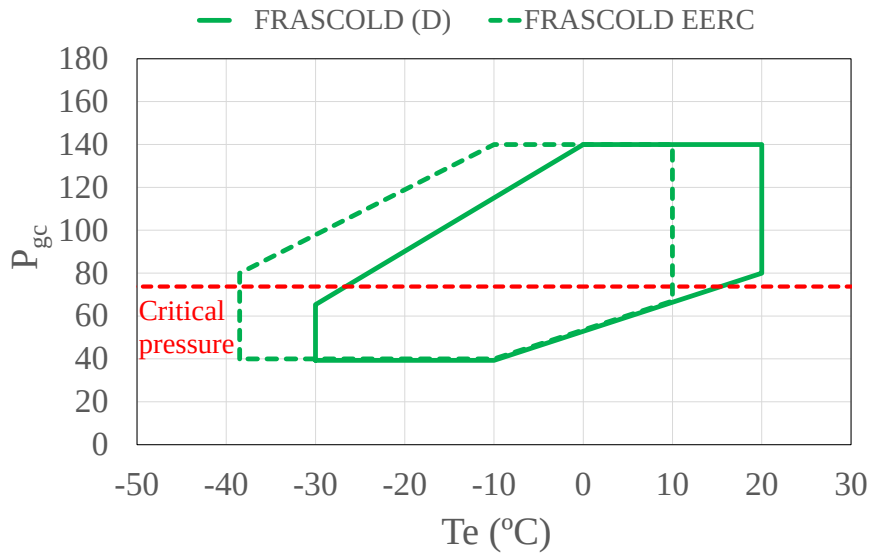

c)

Fig. 4-1. EERC modified envelope: (a) DORIN; (b) GEA; (c) FRASCOLD.

Once the capacity of the EERC to extend the operating limits of commercial compressors for low-temperature refrigeration in warm climates is confirmed, a thermodynamic analysis of the system performance is conducted. Some assumptions are considered in the analysis, such as evaporating temperatures ranging from -10 ºC to -38.5 ºC, that were revealed the minimum values to avoid the triple point inside the ejector. Moreover, the outlet temperature of the gas cooler was set to 35 ºC, as average value of typical conditions in warm climates.

Fig. 4-2.a shows a COP comparison between the EERC and the RC. To assess the influence on the performance, simulations with and without IHX have been conducted. As expected, the COP decreases as the evaporating temperature is reduced. However, a significant improvement can be achieved by the EERC, reaching a COP improvement of 34% without IHX compared to the RC. If the IHX is considered, the COP improvement concerning the RC is 22.7%, reaching a value of COP of 1.2 even in the most unfavorable conditions.

Taking into account that these simulations keep constant the refrigeration capacity, it can be deduced that an electrical consumption reduction is obtained by using the EERC. This fact is appreciable in

Fig. 4-2.b, which represents the specific power absorbed by the compressor in function of the evaporating temperature. The decrease in power consumption is coherent to a pressure ratio reduction. Focusing on the lowest evaporating temperature, a power reduction of 34% is obtained adopting of the EERC, and 22.7% if the IHX is used. This significant improvement suggests that the cost of the compressor used in the EERC will be lower compared to the one used in the RC.

Concerning the gas cooler capacity, Fig. 4-2.c illustrates a normalized comparison of thermal power. As can be appreciated, the use of the EERC allows a 22.7% power dissipation reduction, and 13.4% if the IHX is used. Considering that the lower gas cooler capacity, the lower the investment cost of the component, a cost reduction is expected by the use of the EERC with IHX.

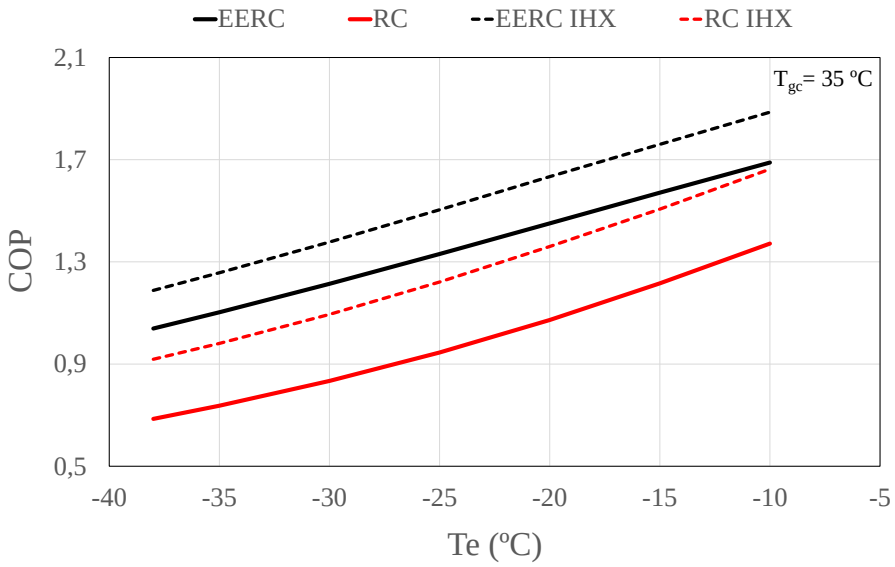

(a)

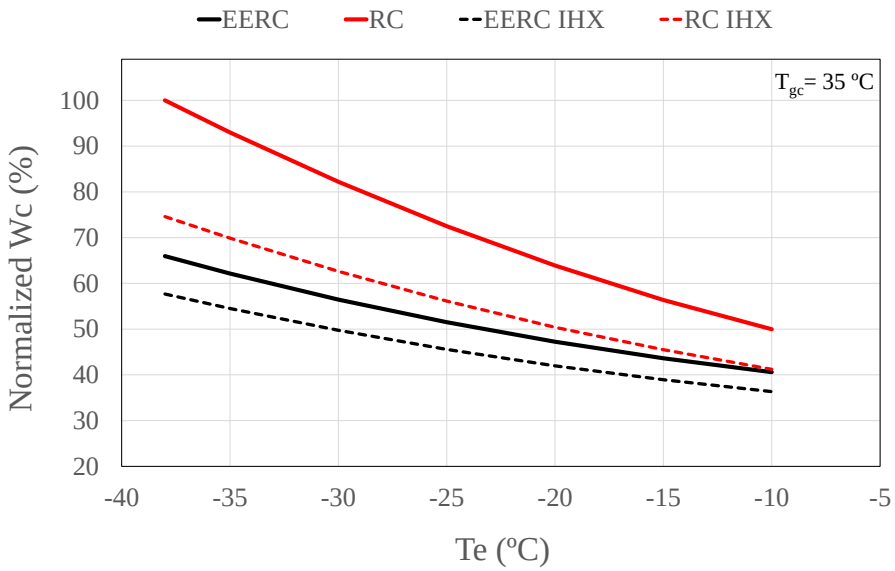

(b)

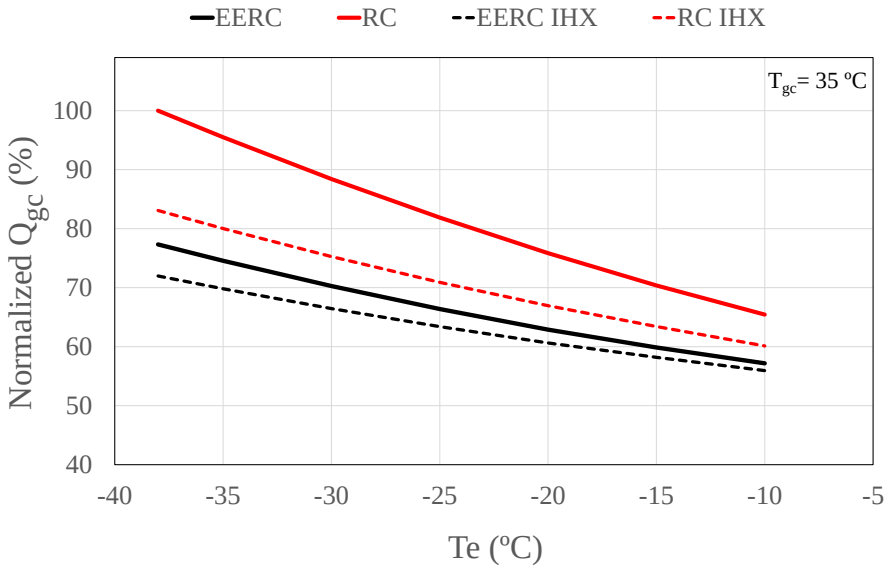

(c)

Fig. 4-2. EERC and RC thermodynamic performance: (a) COP; (b) electric power absorbed by the compressor; (c) gas cooler capacity.

To contribute with information about the ejector performance, the entrainment ratio and the efficiency are analyzed. The entrainment ratio variation along the range of simulation is illustrated in Fig. 4-3.a, which varies from 0.5 without IHX, to 0.7 if the IHX is used. Elbel efficiency is shown in Fig. 4-3.b. As can be appreciated the lower the evaporation temperature the higher the efficiency of the ejector, which is due to the increase of the pressure difference between primary and secondary nozzles. This improvement is produced against the COP, which decreases with the evaporating temperature, requiring an optimization to operate with the most suitable discharge pressure for the whole performance of the cycle. Values of Elbel efficiencies range from 52% without IHX, to 59% using IHX.

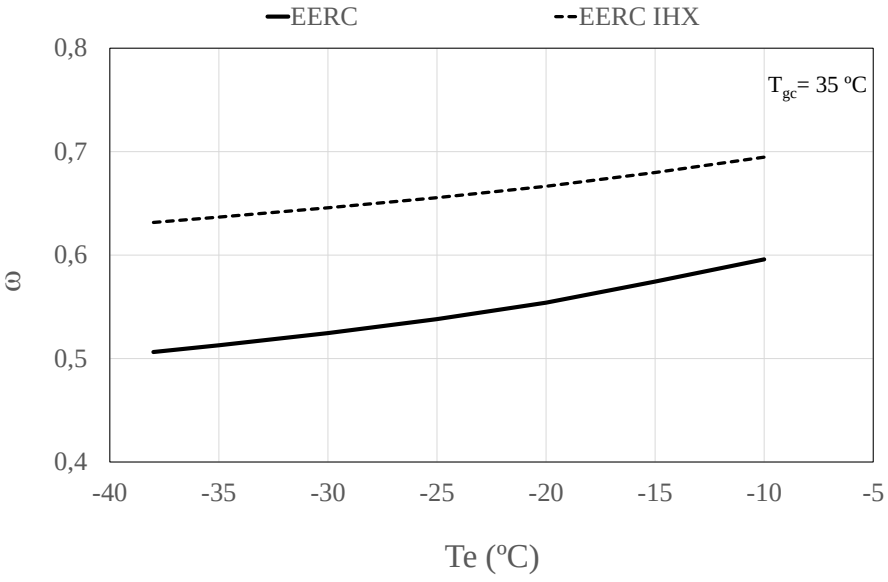

(a)

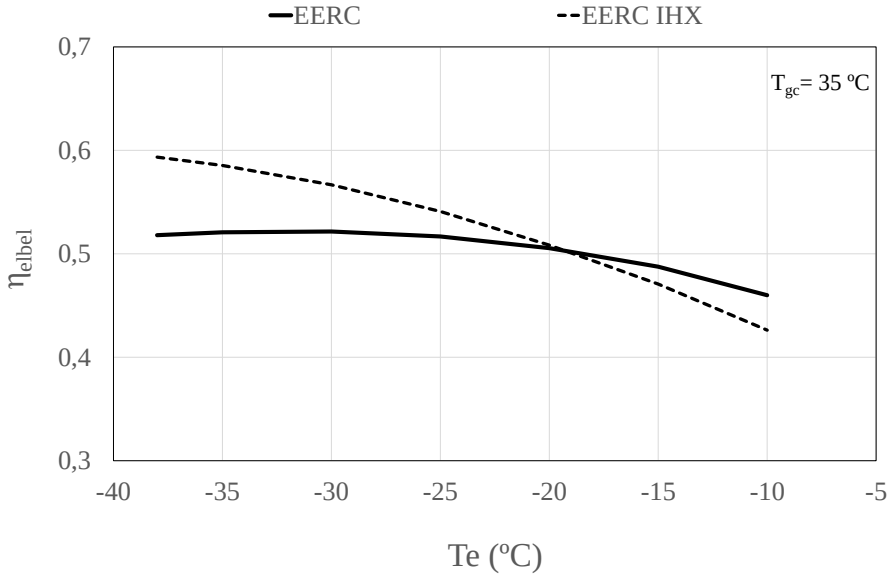

(b)

Fig. 4-3. Ejector parameters analysis: (a) entrainment ratio; (b) Elbel's efficiency.

From the previous analysis, the predicted investment cost of the EERC with regard to the compressor and gas cooler should be lower, since lower powers are required. Nonetheless, the total investment cost should be assessed. The results of the normalized investment costs obtained from the optimization are depicted in Fig. 4-4. The optimization has been conducted to maximize the NPV. Nonetheless, the same results are obtained if the COP is maximized, since the power consumption reduction directly minimizes the yearly power costs. First, this figure shows that the lower the evaporating temperature, the higher the difference between the EERC and the RC, acquiring a great relevance for low-temperature refrigeration applications. For the temperature of -38.5 ºC the EERC total investment cost is 12.6% lower than the RC. The main reason for this improvement is due to the difference in the cost of the compressor, which results in 30% cheaper than the RC. Notice that the compressor used in the EERC requires a lower volume displacement, supports a lower pressure ratio, and requires a lower consumption than the RC. Regarding the cost of the ejector, as expected, the investment required increases for lower evaporating temperatures, since there is a greater pressure difference between the secondary nozzle and the diffuser outlet. However, the cost of the ejector does not have a significant weight on the total investment cost.

The previous analysis has shown the relevance of the EERC for low-evaporating temperatures in warm climates. The analysis was performed in a normalized way, comparing the relative improvement with respect to the reference system. Aiming to provide absolute values of improvement for different power capacities, Fig. 4-5 depicts the NPV evolution over the system lifetime for refrigeration systems from 20 to 80 kW. From a general point of view, the improvement of the EERC is more significant as the power capacity increases. Thus, if the EERC is compared with the RC for a refrigeration capacity of 80 kW, reductions about 20% of the total investment and yearly power costs are achieved. This result is a consequence of a more efficient and economic system for low-temperature refrigeration applications in warm climates.

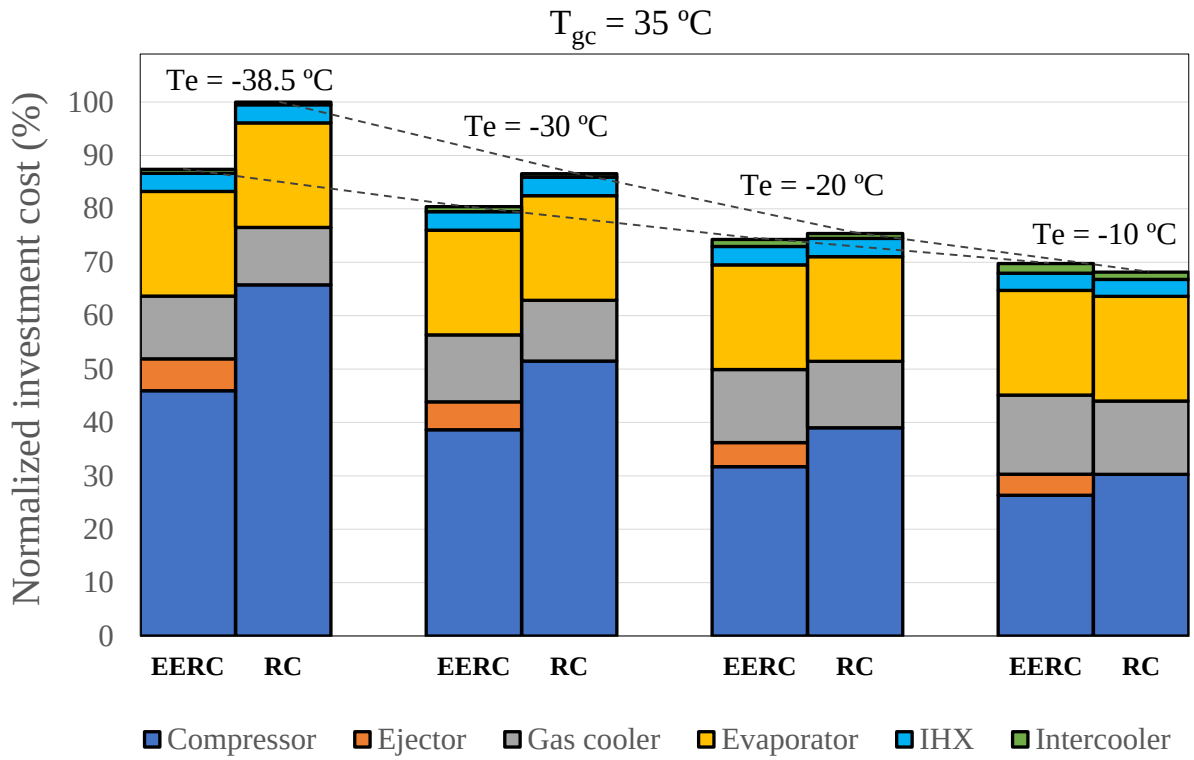

Fig. 4-4. Normalized investment cost optimizing the NPV.

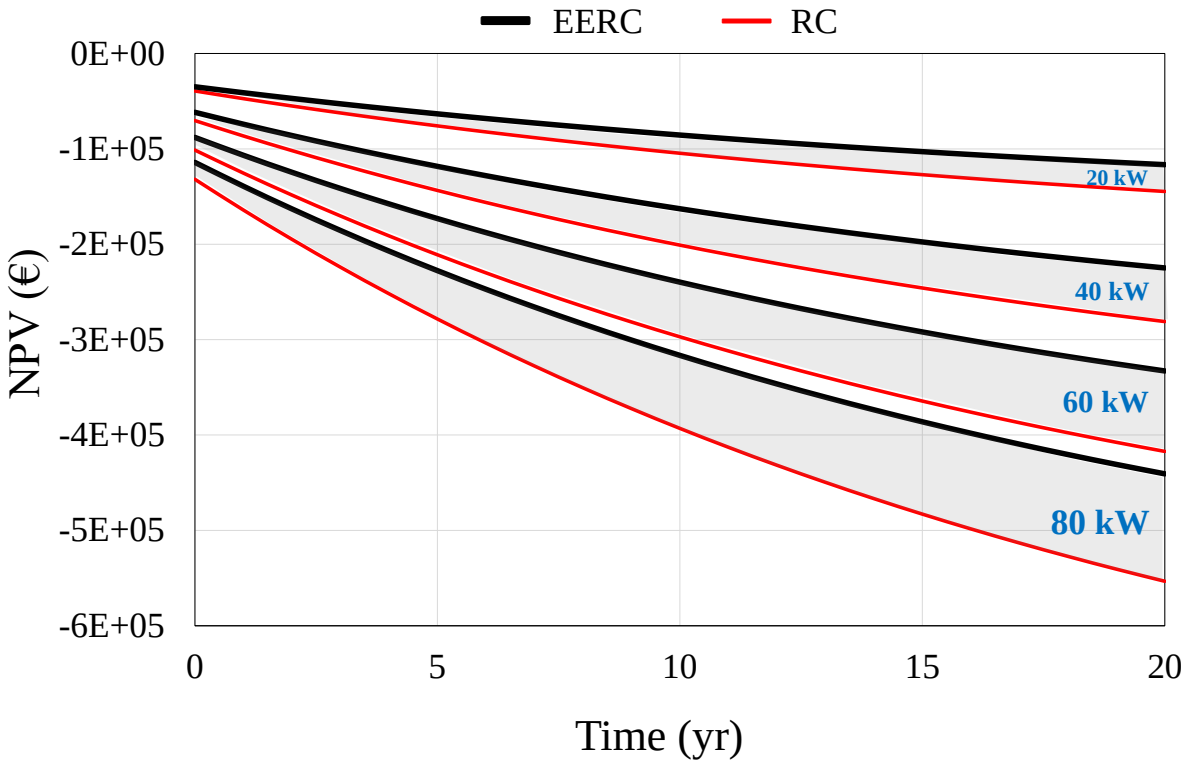

Fig. 4-5. NPV of the EERC and RC cycle for different refrigeration capacities.

5 CONCLUSIONS

This document has analyzed the thermodynamic and economic feasibility of the EERC for low-temperature refrigeration in warm climates. For this, a thermoeconomic model has been developed, considering a two-phase flow ejector, a double-stage compressor with intercooler, and an internal heat exchanger for superheating-subcooling. Special attention has received the compressor, which was developed as a black-box model and that was validated with a suitable accuracy within the operating envelope of the compressor. Cost correlations were used for the economic model, that were obtained from commercial information and equations reported in the literature. Thus, the thermoeconomic optimization was conducted to reach the most cost-effective system.

First, the operating limits of the EERC have been determined. The minimum evaporating temperature reached was -38.5 ºC, which was revealed the borderline to avoid the triple point inside the ejector. The use of the ejector demonstrated that it lifts the suction pressure of the compressor, moving the operating envelope of the compressor to higher discharge pressures, and enabling the operation in warm climates.

Second, a thermodynamic comparison between the EERC and RC performance was conducted. The EERC reached higher values of COP, which are explained by a lower power absorbed due to the compression ratio reduction. In particular, the COP improvement of the EERC using the IHX was 22.7%, reaching a COP of 1.2 at the most unfavorable conditions assessed. Moreover, the gas cooler capacity required was 13.4% lower than the reference cycle using IHX. Thus, a more efficient and compact system can be reached using the EERC for the application analyzed.

Third, the optimization was done to maximize the NPV, providing an equivalent result to that maximizing the value of COP. The results showed that, for the evaporating temperature of -38.5 ºC, the total investment cost of the EERC was 12.6% lower than the RC cost. The main reason for that improvement was revealed due to the difference in the cost of the compressor, which resulted 30% cheaper than the RC, since a lower volume displacement, pressure ratio, and consumption was required by the EERC.

Fourth, the NPV evolution over the system lifetime was studied. The results showed that the improvement of the EERC is more significant as the refrigeration capacity increases, reaching reductions about 20% of the total investment and yearly power costs using an 80 kW EERC.

Finally, as a general conclusion, the EERC adoption for refrigeration temperatures above -38.5 ºC in warm climates has been demonstrated feasible, allowing the use of smaller commercial compressors within a broader operating envelope.

REFERENCES

[1] International Institute for Sustainable Development (IISD), Kigali Amendment, (2019). Available in: < sdg.iisd.org > [accessed: 01.07.2020]

[2] M. Isaac, D.P. van Vuuren, Modeling global residential sector energy demand for heating and air conditioning in the context of climate change, Energy Policy. 37 (2009) 507–521.

[3] A. Barrena Medina, Reglamento (UE) núm. 517/2014 del Parlamento Europeo y del Consejo de 16 de abril de 2014 sobre los gases fluorados de efecto invernadero y por el que se deroga el Reglamento (CE) núm. 842/2006 (DOUE L 150/195, de 20 de mayo de 2014), Actual. Jurídica Ambient. 2014 (2014) 46–46.

[4] GasServei: Especialistas en gases refrigerantes, Reglamento Europeo No517-2014 (Implicaciones a corto y medio plazo), (2014) 1–9.

[5] J.S. Jadhav, A.D. Apte, Review of Cascade Refrigeration System with Different Refrigerant Pairs, Novat. Publ. Int. J. Innov. Eng. Res. Technol. [Ijiert]. 2 (2015) 74–81.

[6] D.K. Ramesha, S. Kiran, K. Kushal, An Overview of Propane Based Domestic Refrigeration Systems, Mater. Today Proc. 5 (2018) 1599–1606.

[7] B. Holling, C. Kandziora, R. Ritter, CO2 recovery from industrial hydrogen facilities and steel production to comply with future European Emission regulations, Energy Procedia. 37 (2013) 7221–7230.

[8] B. Yu, J. Yang, D. Wang, J. Shi, J. Chen, An updated review of recent advances on modified technologies in transcritical CO2 refrigeration cycle, Energy. 189 (2019) 116147.

[9] Y. Yerdesh, Z. Abdulina, A. Aliuly, Y. Belyayev, M. Mohanraj, A. Kaltayev, Numerical simulation on solar collector and cascade heat pump combi water heating systems in Kazakhstan climates, Renew. Energy. 145 (2020) 1222–1234.

[10] P. Gullo, Innovative fully integrated transcritical R744 refrigeration systems for a HFC-free future of supermarkets in warm and hot climates, Int. J. Refrig. 108 (2019) 283–310.

[11] P. D'Agaro, G. Cortella, A. Polzot, R744 booster integrated system for full heating supply to supermarkets, Int. J. Refrig. 96 (2018) 191–200.

[12] P. Gullo, K. Tsamos, A. Hafner, Y. Ge, S.A. Tassou, State-of-the-art technologies for transcritical R744 refrigeration systems - A theoretical assessment of energy advantages for European food retail industry, Energy Procedia. 123 (2017) 46–53.

[13] P. Gullo, A. Hafner, G. Cortella, Multi-ejector R744 booster refrigerating plant and air conditioning system integration – A theoretical evaluation of energy benefits for supermarket applications, Int. J. Refrig. 75 (2017) 164–176.

[14] K. Zolcer Skačanová, M. Battesti, Global market and policy trends for CO2 in refrigeration, Int. J. Refrig. 107 (2019) 98–104.

[15] S. Elbel, N. Lawrence, Review of recent developments in advanced ejector technology, Int. J. Refrig. 62 (2016) 1–18.

[16] F. Santini, G. Bianchi, D. Di Battista, C. Villante, M. Orlandi, Experimental investigations on a transcritical CO2 refrigeration plant and theoretical comparison with an ejector-based one, Energy Procedia. 161 (2019) 309–316.

[17] Z. Jin, A. Hafner, T.M. Eikevik, P. Nekså, Preliminary study on CO 2 transcritical ejector enhanced compressor refrigeration system for independent space cooling and dehumidification, Int. J. Refrig. 100 (2019) 13–20.

[18] K. Zolcer Skačanová, G. Anti, Technical report on energy efficiency in HFC-free supermarket refrigeration, (2018).

[19] Hengel, Difference between freezing and deep freezing, 33 (2017).

[20] T. Lucas, A.L. Raoult-Wack, Immersion chilling and freezing in aqueous refrigerating media: Review and future trends, Int. J. Refrig. 21 (1998) 419–429.

[21] H.T. Walnum, T. Andresen, K. Widell, Dynamic simulation of batch freezing tunnels for fish using Modelica, Procedia Food Sci. 1 (2011) 698–705.

[22] I. Tolstorebrov, T.M. Eikevik, M. Bantle, Effect of low and ultra-low temperature applications during freezing and frozen storage on quality parameters for fish, Int. J. Refrig. 63 (2016) 37–47.

[23] G. Di Nicola, F. Polonara, R. Stryjek, A. Arteconi, Performance of cascade cycles working with blends of CO2 natural refrigerants, Int. J. Refrig. 34 (2011) 1436–1445.

[24] T.S. Lee, C.H. Liu, T.W. Chen, Thermodynamic analysis of optimal condensing temperature of cascade-condenser in CO2/NH3 cascade refrigeration systems, Int. J. Refrig. 29 (2006) 1100–1108.

[25] S. Eini, H. Shahhosseini, N. Delgarm, M. Lee, A. Bahadori, Multi-objective optimization of a cascade refrigeration system: Exergetic, economic, environmental, and inherent safety analysis, Appl. Therm. Eng. 107 (2016) 804–817.

[26] N. Purohit, D.K. Gupta, M.S. Dasgupta, Energetic and economic analysis of trans-critical CO2 booster system for refrigeration in warm climatic condition, Int. J. Refrig. 80 (2017) 182–196.

[27] C. Amaris, K.M. Tsamos, S.A. Tassou, Analysis of an R744 typical booster configuration, an R744 parallel-compressor booster configuration and an R717/R744 cascade refrigeration system for retail food applications. Part 1: Thermodynamic analysis, Energy Procedia. 161 (2019) 259–267.

[28] Z. Huang, H. Zhao, Z. Yu, J. Han, Simulation and optimization of a R744 two- temperature supermarket refrigeration system with an ejector, Int. J. Refrig. 90 (2018) 73–82.

[29] J. Catalán-Gil, D. Sánchez, R. Llopis, L. Nebot-Andrés, R. Cabello, Energy evaluation of multiple stage commercial refrigeration architectures adapted to F-gas regulation, Energies. 11 (2018).

[30] J. qiang Deng, P. xue Jiang, T. Lu, W. Lu, Particular characteristics of transcritical CO2 refrigeration cycle with an ejector, Appl. Therm. Eng. 27 (2007) 381–388.

[31] M. Yari, Performance analysis and optimization of a new two-stage ejector-expansion transcritical CO2 refrigeration cycle, Int. J. Therm. Sci. 48 (2009) 1997–2005.

[32] T. Bai, G. Yan, J. Yu, Thermodynamic analyses on an ejector enhanced CO2 transcritical heat pump cycle with vapor-injection, Int. J. Refrig. 58 (2015) 22–34.

[33] X. Liu, R. Fu, Z. Wang, L. Lin, Z. Sun, X. Li, Thermodynamic analysis of transcritical CO2 refrigeration cycle integrated with thermoelectric subcooler and ejector, Energy Convers. Manag. 188 (2019) 354–365.

[34] L. Cecchinato, M. Chiarello, M. Corradi, E. Fornasieri, S. Minetto, P. Stringari, C. Zilio, Thermodynamic analysis of

different two-stage transcritical carbon dioxide cycles, Int. J. Refrig. 32 (2009) 1058–1067.

[35] Y. Chen, H. Zou, J. Dong, H. Xu, C. Tian, D. Butrymowicz, Experimental investigation on refrigeration performance of a CO2 system with intermediate cooling for automobiles, Appl. Therm. Eng. 174 (2020) 115267.

[36] F.E. Manjili, M.A. Yavari, Performance of a new two-stage multi-intercooling transcritical CO 2 ejector refrigeration cycle, Appl. Therm. Eng. 40 (2012) 202–209.

[37] D. Wang, Z. Chen, Z. Gu, Y. Liu, Z. Kou, L. Tao, Performance analysis and comprehensive comparison between CO2 and CO2/ethane azeotropy mixture as a refrigerant used in single-stage and two-stage vapor compression transcritical cycles, Int. J. Refrig. 115 (2020) 39–47.

[38] Z. Zhang, X. Feng, D. Tian, J. Yang, L. Chang. Progress in ejector-expansion vapor compression refrigeration and heat pump systems. Energy Conversion and Management 207 (2020) 112529.

[39] J.A. Expósito-Carrillo, F.J. Sánchez de La Flor, J.M. Salmerón-Lissén. Thermodynamic comparison of ejector cooling cycles. Ejector characterisation by means of entrainment ratio and compression efficiency. international journal of refrigeration 74 (2017) 371–384.

[40] H. Zhang, L. Wang, L. Jia, X. Wang. Assessment and prediction of component efficiencies in supersonic ejector with friction losses. Applied Thermal Engineering 129 (2018) 618–627.

[41] M.M. Petrovic, V.D. Stevanovic. Two-Component Two-Phase Critical Flow. FME Transactions (2016) 44, 109-114 - 109.

[42] W. Angielczyk; Y. Bartosiewicz; D. Butrymowicz, JM. Seynhaeve. 1-D Modeling Of Supersonic Carbon Dioxide Two-Phase Flow Through Ejector Motive Nozzle. International Refrigeration and Air Conditioning Conference, 2010. Paper 1102.

[43] Lund H, Flatten T. Equilibrium conditions and sound velocities in two-phase flows. In: Proceedings of the SIAM annual meeting. Pittsburgh: SIAM; 2010. p. 1–5.

[44] J.M. Cardemil, S. Colle. A general model for evaluation of vapor ejectors performance for application in refrigeration. Energy Conversion and Management 64 (2012) 79–86.

[45] J. Anderson. Modern compressible flow. 2nd ed. New York: McGraw-Hill; 2002.

[46] S. Elbel, P. Hrnjak, Experimental validation of a prototype ejector designed to reduce throttling losses encountered in transcritical R744 system operation, Int. J. Refrig. 31 (2008) 411–422.

[47] DORIN software version 19.10. Available in: <www.dorin.com> [accessed: 01.07.2020].

[48] Güntner software of dry cooling technology GPC 2020. Available in: <www.guentner.eu> [accessed: 01.07.2020].

[49] S. Khanmohammadi, M. Goodarzi, S. Khanmohammadi, H. Ganjehsarabi, Thermoeconomic modeling and multi-objective evolutionary-based optimization of a modified transcritical CO2 refrigeration cycle, Therm. Sci. Eng. Prog. 5 (2018) 86–96.

[50] S. Sanaye, M. Emadi, A. Refahi, Thermal and economic modeling and optimization of a novel combined ejector refrigeration cycle, Int. J. Refrig. 98 (2019) 480–493.

[51] B. Peris Pérez, Thermo-economic assessment of small-scale organic Rankine cycle for low-grade industrial waste heat recovery based on an experimental application, (2017) 237.